PIBB 生物化学与生物物理进展
Progress in Biochemistry and Biophysics
2022,49(10):2015~2023
www.pibb.ac.cn

Intracellular Photoacoustic Imaging Using Folate Receptor Targeting Gold Nanorods*

ZHONG Jun-Ping[1)**], CHEN Jin-Ying[2)**]

([1)]*Guangdong-Hong Kong-Macao Joint Laboratory for Intelligent Micro-Nano Optoelectronic Technology, School of Physics and Optoelectronic Engineering, Foshan University, Foshan* 528225, China;

[2)]*Department of Ophthalmology, the First Affiliated Hospital of Jinan University, Guangzhou* 510632, China)

Abstract **Objective** Molecular imaging technology has the characteristic of "early detection", since aberrations at molecular levels occur much earlier than the changes at the anatomical level. In this study, intracellular photoacoustic molecular imaging (PMI) method was used to map the folic-acid-conjugated gold nanorods (FA-AuNRs) targeted on cancer cells. **Methods** We synthesized the FA-AuNRs and studied their properties including morphology, absorption spectrum, and biocompatibility. The conjugated folic acid has endowed the FA-AuNRs with the ability to target folate-receptor-expressing cancer cells. Then, PMI experiment was performed to study the target specificity of FA-AuNRs on cancer cells. **Results** FA-AuNRs were rod-shaped with a near-infrared absorption peak at ~800 nm. We observed the strong photoacoustic signals in the cytoplasm of cancer cells, while weak photoacoustic signals in the normal cells, indicating the selective uptake of FA-AuNRs inside cancer cells *via* folate-receptor-mediated endocytosis. The study demonstrated the ability of PMI to precisely map the FA-AuNRs targeted on cancer cells. **Conclusion** With the aid of specific targeting, information about the surface molecules of cancer cells can be obtained by PMI. This method is expected to visualize, characterize and quantify biological processes at cellular and molecular levels.

Key words molecular imaging, nanoparticle, gold nanorods, photoacoustic imaging
DOI: 10.16476/j.pibb.2022.0136

Photoacoustic imaging is a non-invasive biomedical imaging technology with high resolution and high contrast[1-3]. In photoacoustic imaging, the pulsed laser is absorbed by the targets and converted into heat, which causes transient thermoelastic expansion and broadband ultrasound emission[4-6]. The generated ultrasonic waves are detected by an ultrasonic transducer and then analyzed to produce a photoacoustic image. The photoacoustic imaging technique has been successfully applied to the early diagnosis of tumor angiogenesis, brain functional imaging, molecular imaging, and nanotherapeutic evaluation[7-10]. At present, two types of photoacoustic systems have been developed, photoacoustic computed tomography (PAT) and photoacoustic microscopy (PAM). A typical PAT system usually uses a large unfocused light spot to illuminate the sample and multi-element detector array to acquire photoacoustic signals. The PAM system uses an optical objective lens to focus light into biological tissues and a spherically focused ultrasound detector with two-dimensional (2D) point-by-point scanning[11-12]. However, to determine the position of the probe, PAM allows a higher spatial resolution than PAT.

* This work was supported by grants from The National Natural Science Foundation of China (61705036), the Fundamental Research Funds for the Central Universities (21621052), Medical Scientific Research Foundation of Guangdong Province, China (A2022415), and the Research Fund of Guangdong-Hong Kong-Macao Joint Laboratory for Intelligent Micro-Nano Optoelectronic Technology (2020B1212030010).

** Corresponding author.
ZHONG Jun-Ping. Tel:86-13268286089, E-mail: zjp85@126.com
CHEN Jin-Ying. Tel:86-15017541741, E-mail: chenjy0907@126.com

Received: April 2, 2022 Accepted: June 30, 2022

Molecular imaging uses imaging techniques to display specific molecules at the tissue, cellular, and subcellular levels to reflect changes at the molecular level, achieves the purpose of displaying the biological process at the molecular and cellular levels[13-15]. Compared with classical medical imaging technology, molecular imaging technology has the characteristic of "early detection." The classical imaging technologies (*e. g.*, X-ray, CT, MRI, and ultrasound) mainly show the final effect of molecular changes[13-17]. For example, although the final anatomical changes in organs owing to a disease can be observed, the prior molecular changes cannot be detected. Molecular imaging technologies can detect abnormalities at the cellular and molecular levels in the process of disease, before anatomical changes occur[13-15]. As a bridge between molecular biology and clinical medicine, molecular imaging has great potential in the early detection and effective treatment of diseases[16-17]. Currently, major optical imaging modalities capable of providing cellular and molecular information of cancer are fluorescence molecule imaging (FMI), optical coherence tomography molecular imaging (OCTMI) and photoacoustic molecular imaging (PMI)[6, 10, 15-17]. PMI uses nanoprobes as targeting agents to detect specific biomarkers *in vitro* and *in vivo*[13]. As summarized in Table 1, compared with FMI and OCTMI, PMI has a deeper imaging depth (up to 5−6 cm) due to the much weaker scattering of ultrasonic signals than light in tissue[6, 10, 15-17]. PMI does not rely on fluorescence emission of molecules, giving it the ability to image nearly all molecules[15-17]. Moreover, PMI can be easily combined with ultrasound imaging because both systems can share the same detector and electronics[8-9].

Table 1 Summary of the optical molecular imaging methods of previously reported

Methods	Imaging principle	Features	References
Photoacoustic molecular imaging (PMI)	By converting laser into ultrasound emission	(1) PMI provides high spatial resolution determined by the focusing optical beams (~1 μm) (2) Deep imaging depth (up to 5−6 cm) (3) PMI does not rely on fluorescence emission of molecules, giving it the ability to image nearly all molecules	[1-2,6-7, 10-17]
Fluorescence molecular imaging (FMI)	Imaging of fluorescent agents engineered to target specific disease biomarkers	(1) FMI achieves micrometre-scale resolution (~200 nm) (2) Penetration depth (1−2 mm) (3) Rely on fluorescence emission of molecules	[15-17]
Optical coherence tomography molecular imaging (OCTMI)	Created from backscattering light in target tissue	(1) Spatial resolution (1−10 μm) (2) Penetration depth (1−2 mm) (3) Limited capabilities to perform molecular imaging due to the high background signal for molecular imaging	[1,6, 10,16]

The AuNRs have many unique photophysical properties and have been widely used for target-specific cancer diagnosis and therapy[18-22]. AuNRs have multiple advantages. (1) AuNR is easy to synthesize. It exhibit surface modification capabilities to improve the clinical outcome[23-24]. (2) AuNR has excellent surface plasmon resonance in the near-infrared (NIR) range. Thus, it is easy to tune to the region of maximum light transmission through tissues[23-24]. (3) At the same molar concentration, the light absorbance of AuNRs is ~160 times higher than single-walled carbon nanotubes, and ~5 000 times higher than indocyanine green[13]. (4) AuNRs efficiently convert absorbed energy into heat and then generate strong photoacoustic waves[13, 25]. As the uptake amount of AuNRs in cells plays an important role in diagnosis and therapy, the high-resolution visualization of the uptake and distribution of AuNRs is important, especially in the study of intracellular metabolism.

In this study, folic acid (FA) conjugated AuNRs (FA-AuNRs) were used as nanoprobes for PMI to map the folate receptor (FR). The FR is overexpressed in many cancers, including brain, lung, breast, and ovarian cancers, whereas the expression in most normal tissues is low to negligible[26-28]. It is a promising candidate for the selective delivery of anticancer drugs to FR-expressing tumors[26].

Introducing FA into the FA-AuNRs can improve the specificity, penetration, and distribution of a drug in FR-expressing tumors. Herein, the properties of FA-AuNRs (including morphology and absorption spectrum) are studied. The photoacoustic effect of FA-AuNRs was also investigated. By functionalizing with FA, the nanoprobes can selectively enter cancer cells that overexpress FRs on the cell membrane. Then, the target specificity of these FA-AuNRs was evaluated *in vitro* by PAM.

1 Materials and methods

1.1 Materials

Amine-PEG-Thiol (HS-PEG-NH_2, MW 4 000) was purchased from Avanti Polar Lipids Inc. (AL, USA). Cell counting kit-8 (CCK-8) was purchased from Dojindo Laboratories (Kumamoto, Japan). FA was purchased from Sigma-Aldrich Co. (MO, USA). All of the reagents were used without further purification.

1.2 Preparation of FA−AuNRs nanoparticles

FA-AuNRs nanoparticles were prepared following the procedures of our previous study[13].

1.3 Characterization experiments

An ultraviolet/visible (UV-Vis) spectrometer (Lambda 35, Perkin-Elmer, MA, USA) was used to create the absorption spectrum. A JEM-100CXII (Jeol Inc., Tokyo, Japan) transmission electron microscope was used to study the morphology and size of FA-AuNRs with 70 pA current and 100 kV voltage.

1.4 Cell culture

HeLa cells were maintained in Dulbecco's modified Eagle's medium (Gibco) supplemented with 10% fetal bovine serum, penicillin (100 units/ml), and streptomycin (100 mg/L) in a 5% CO_2 humidified incubator at 37℃. As FA-starved cells overexpress FRs on the cell membrane surface, HeLa cells were cultured in an FA-free medium. The cells were passaged for at least 4 times in the FA-free medium before use to ensure overexpression of FR on the surface of HeLa cells.

1.5 Determination of cytotoxicity

HeLa cells were seeded in 96-well culture plates (5×10^3 cells/well, 100 μl). After being incubated with the FA-AuNRs nanoprobes for 2 h, the cells were then rinsed with phosphate buffer solution (PBS) 3 times. Cell cytotoxicity was assessed with CCK-8 at 24 h after the laser irradiation. A_{450}, the absorbance value at 450 nm, was read with a 96-well plate reader (INFINITEM200, Tecan, Switzerland) to determine the viability of the cells.

1.6 Confocal laser scanning microscopy

1×10^4 cells were seeded on 35-mm Petri dishes, then incubated with 0.3 nmol/L fluorescein isothiocyanate (FITC)-labeled FA-AuNRs. After incubation, cells were rinsed with PBS 3 times and the medium was replaced with fresh medium. Fluorescence was monitored using a commercial laser scanning microscope (LSM510/ConfoCor2) combination system (Zeiss, Jena, Germany) equipped with a Plan-Neofluar 40/1.3 numerical aperture oil differential interference contrast objective. FITC was excited at 488 nm using an argon laser, and the emitted fluorescent light was collected using an LP 500 filter.

1.7 Statistical analysis

Each experiment was repeated at least 3 times. Significant differences between groups were determined using the Student's *t*-test (two-tailed). Quantitative data were expressed as mean ± standard deviation (SD). Otherwise, representative data are shown.

2 Results

2.1 Characterization of the FA−AuNRs

AuNRs have two peaks in the optical absorption spectral analysis. One is in the visible region of 520−530 nm and the other is in the NIR region near 800 nm (Figure 1a). UV-Vis spectra revealed that FA-AuNRs absorption spectra exhibit maxima of FA and AuNRs, confirming the successful FA conjugation with AuNRs. Compared to AuNRs, the absorption spectra of the FA-AuNRs probe were red-shifted by approximately 20 nm. Figure 1b showed a typical transmission electron microscopy image of FA-AuNRs, which were rod-shaped with average dimensions of 9−11 nm in diameter and a length of 40−70 nm.

2.2 Toxicity evaluation of the AuNRs

The CCK-8 assay showed that the cytotoxicity of FA-AuNRs depended on its concentration. A cell viability of ~94.7% was observed at 0.3 nmol/L and

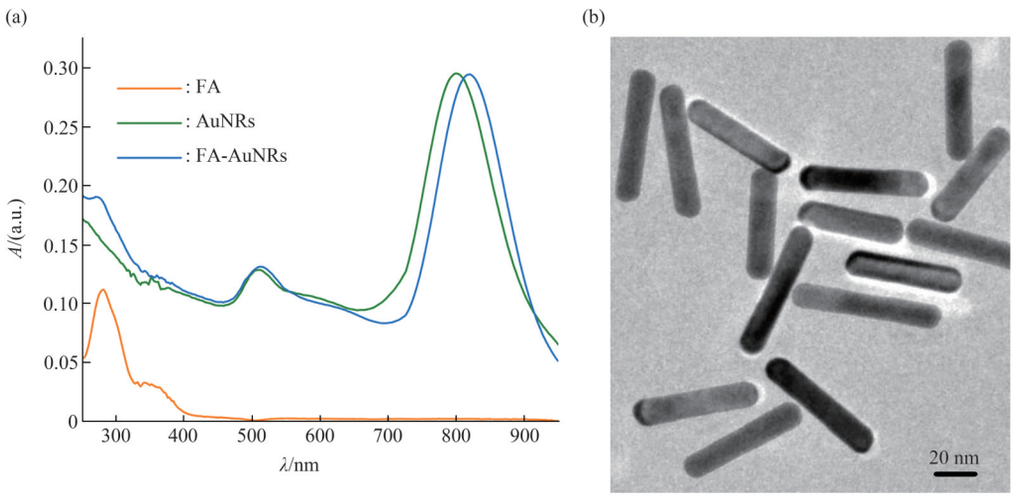

Fig. 1　Characterization of the FA−AuNRs

(a) UV-Vis absorption spectra of FA, AuNRs, and FA-AuNRs. (b) Transmission electron microscopy (TEM) imaging of FA-AuNRs. FA, folic acid. AuNR, gold nanorod. FA-AuNR, folic-acid-conjugated gold nanorod.

no apparent adverse effects were observed at low doses (Figure 2). Thus, as expected, the FA-AuNRs nanoprobe was nontoxic and biocompatible at low doses.

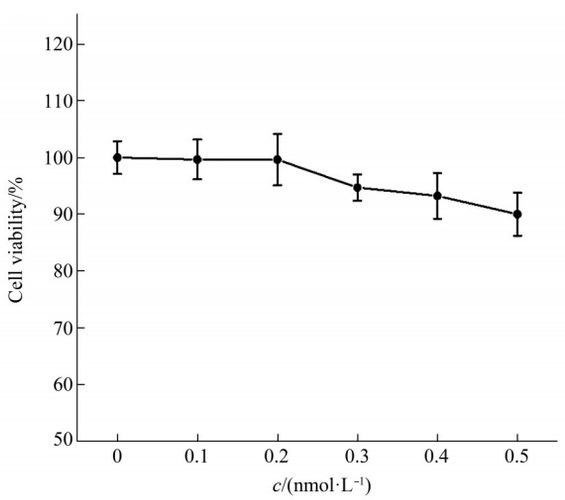

Fig. 2　Cell viability of HeLa cells after incubation with FA−AuNRs

No apparent adverse effects were observed at low doses.

2.3　Photoacoustic imaging system

The schematic of the home-made PAM system is shown in Figure 3. An optical parametric oscillator (OPO) (Surelite II-20, Continuum, Santa Clara, CA, USA) was used to generate 10 ns pulses at 20 Hz. The OPO operated at 800 nm (~5 mJ/cm^2) was used to irradiate the samples in photoacoustic analysis. The laser beam was first passed through a spatial filter and scanned by a 2D scanning galvanometer (6231H, Cambridge Technology, Inc.) in a small imaging field of view (125 μm×125 μm) to delineate the 2D photoacoustic images and show the distribution of FA-AuNRs. The 2D scanning galvanometer triggered by the signals of the laser, was controlled by a computer. Then, the laser beam was focused by a plane microscope objective lens to illuminate the surface of the cells (in the 35 mm glass-bottomed dishes). A photodiode detector was used to monitor the intensity of the laser for calibration of the laser beam. The slide was held by a sample holder mounted onto an *x*, *y*, *z* manual translational stage, that is placed atop the focused ultrasonic transducer (Guangzhou Doppler Electronic Tech. Co., Ltd, China). The transducer (with a center frequency of 15 MHz and a −6 dB bandwidth of 100%) was set on the opposing side of the sample to form the confocal mode of laser and ultrasound. The photoacoustic signal was first amplified with an amplifier (ZFL-500, Minicircuits) and then digitized by a dual-channel data acquisition card NI 5122 at a sampling rate of

100 Msamples/s. Finally, the photoacoustic signal was recorded in a personal computer synchronized to the laser. The photoacoustic signal was averaged 3 times at each scanning grid point to increase the signal to noise ratio. The bright-field images were captured using an intensity controlled white light-emitting diode and the complementary metal-oxide-semiconductor camera.

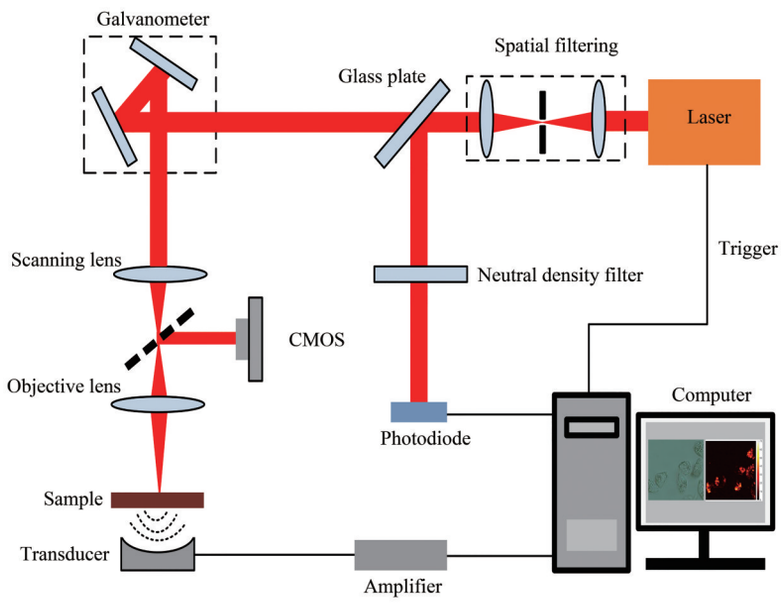

Fig. 3　Schematic diagram of the PAM system

PAM, photoacoustic microscopy. CMOS, complementary metal-oxide-semiconductor.

2.4　Photoacoustic imaging of FA−AuNRs

The photoacoustic signal amplitudes generated by the FA-AuNRs nanoparticles at various concentrations were measured. As shown in Figure 4, the intensity of the photoacoustic signal was observed to be linearly dependent on the concentrations (R^2= 0.985 84).

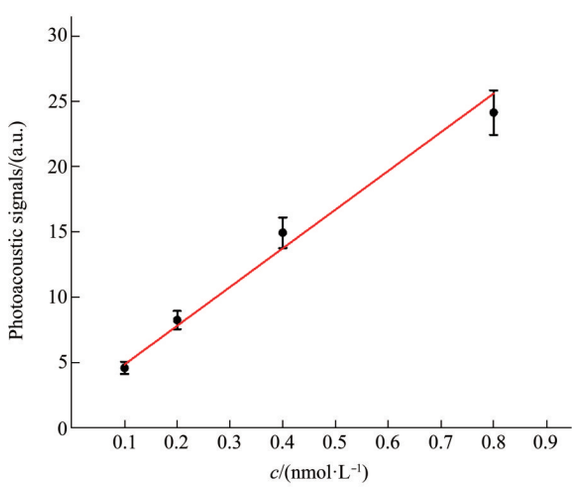

Fig. 4　Photoacoustic signals of FA−AuNRs nanoparticles at various concentrations

The intensity of the photoacoustic signal was observed to be linearly dependent on the concentrations (R^2=0.985 84).

Then, *in vitro* experiments were performed to measure the targeting ability of FA-AuNRs on HeLa cells (a cancer cell line overexpressing FR) as a cancer cell model. The photoacoustic signals were examined using the PAM system, the excited wavelengths of FA-AuNRs in cells corresponded to the peak absorption wavelengths. The bright-field image showed the typical morphology of the cancer cells (Figure 5a). There was no noticeable photoacoustic signals in the HeLa cells without FA-AuNRs incubation (Figure 5b). Figure 5c is the bright field microscope of HeLa cells incubating with AuNRs. Weak photoacoustic signals were observed in the HeLa cells (Figure 5d), indicating the little or no uptake of AuNRs. Figure 5e is the bright field microscope of HeLa cells incubating with FA-AuNRs. The strong photoacoustic signals were observed in the cytoplasm (Figure 5f), indicating that the FA-AuNRs had been in the cells. The results indicated that, FA

targeting significantly increased FA-AuNRs binding to folate receptor-expressing HeLa cells. In addition, the distribution of FA-AuNRs in the cytoplasm can be easily distinguished, as a weak photoacoustic intensity in the cell nucleus (marked with arrows in Figure 5f). Quantitative analysis of photoacoustic signal amplitudes showed that the overall photoacoustic signal intensity level of the HeLa+FA-AuNRs groups was generally very high (Figure 5g), which validated the high concentration of intracellular FA-AuNRs.

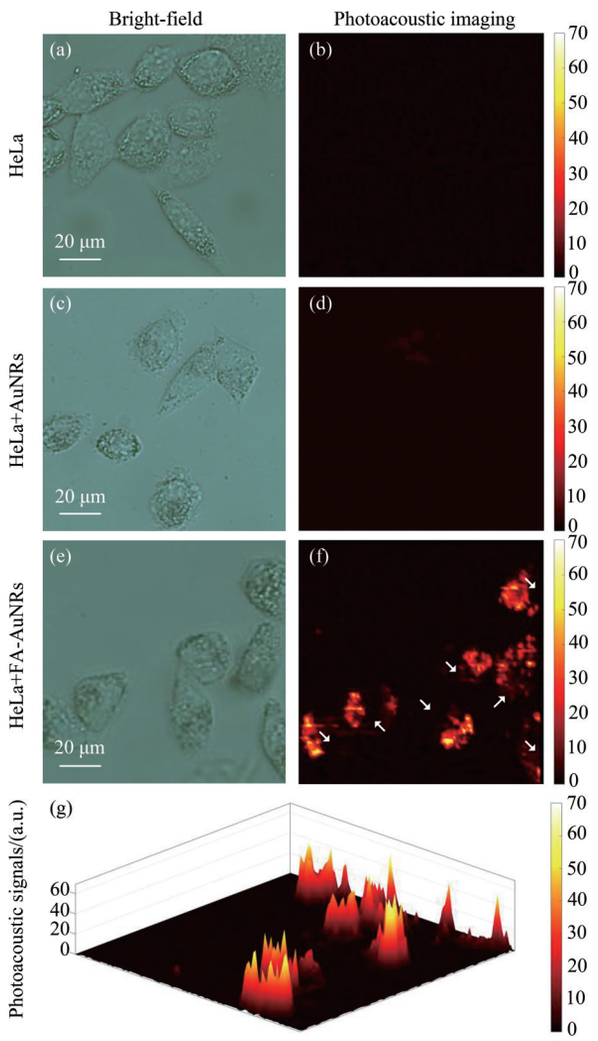

Fig. 5 Photoacoustic imaging of cancer cells

Bright-field microscopy images or representative PAM images of HeLa cells (a, b), AuNR-treated HeLa cells (c, d) or FA-AuNR-treated HeLa cells (e, f). Quantitative analysis of photoacoustic signal intensity of the FA-AuNRs-treated HeLa cells (g).

In order to further confirm the target specificity, NIH-3T3 cells (as a normal cell model) with low FR expression were also incubated with FA-AuNRs. The bright-field images show the typical morphology of the NIH-3T3 cells (Figure 6a). Weak photoacoustic signals were observed in the normal cells (Figure 6b), indicating the little or no uptake of FA-AuNRs. All the results showed that PAM is successfully used to study the selective uptake of FA-AuNRs inside cancer cells.

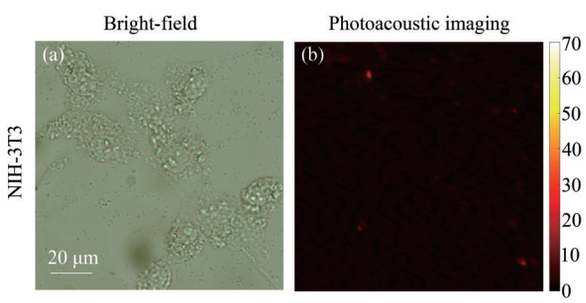

Fig. 6 Photoacoustic imaging of normal cells

(a) Bright-field microscopy image of FA-AuNR-treated NIH-3T3 cells. (b) Representative PAM images of FA-AuNR-treated NIH-3T3 cells.

To confirm target specificity, we used confocal microscopy to investigate the uptake of FITC-labeled FA-AuNRs in cancer cells and normal cells. Strong fluorescence was observed in the cytoplasm (Figure 7, top panel), indicating the presence of FA-AuNRs in the cancer cells. FA-AuNRs did not translocate into the nucleus, as weak fluorescence in the nucleus. Little fluorescence inside cells showed low uptake level of FA-AuNRs into normal cells (Figure 7, bottom panel). The results shown that FA-AuNRs was able to target cancer cells. Overall, the upregulation of FA-AuNRs, evidenced by fluorescence images, agrees with the corresponding PAM images.

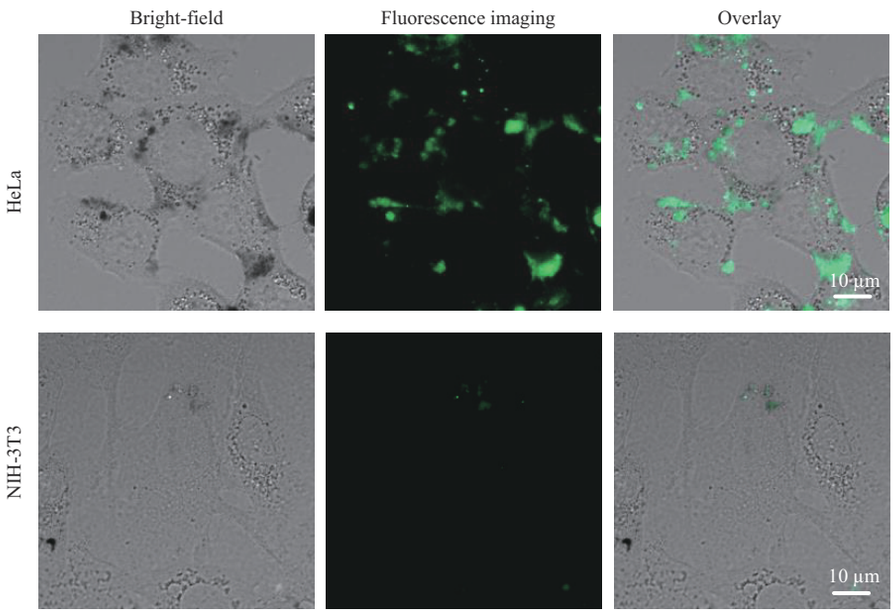

Fig. 7　Confocal images of HeLa cells and NIH−3T3 cells after incubation with the FITC−labeled FA−AuNRs under different treatments

FITC, fluorescein isothiocyanate.

3　Discussion

FA is a promising candidate for cancer cell targeting, because FR is a useful target for the selective delivery of nanoparticles to FR-expressing tumors. The FA-AuNRs were able to enter into the cancer cells *via* ligand-receptor mediated endocytosis pathways[13, 26-28]. The FA-AuNRs effectively target FR-expressing tumor cells, which increase drug accumulation in the tumor region. In this study, FA-AuNRs in cells were visualized by the developed PAM system. The results demonstrated the potential of PAM for the detection of specific targeting nanoparticles. Additionally, by increasing the laser energy, photoacoustic effects can be used to ablate individual cells locally[13]. Laser-induced photoacoustic effects at relatively low laser energy can be used for noninvasive diagnostics, whereas increased laser energy can be used for therapy, such as ablating individual[8, 13]. FA-AuNRs are naturally multifunctional, which can be simultaneously used as imaging and therapeutic agents for both diagnostics and therapy.

The photoacoustic amplitude (A_{PA}) generated after thermoacoustic excitation is described in following equation[29]:

$$A_{PA} = K\sigma_{abs}N_pTP_{laser} + n_{PA} \quad (1)$$

where K represents a constant factor including Grueneisen parameter, heat conversion percentage, and other minor contributors. σ_{abs} is the optical absorption coefficient of the photoabsorber, N_p represents the particle count inside the detection volume, T represents the percentage that light transmits through the beam sampler, P_{laser} represents the laser power and n_{PA} represents the background noise. According to equation (1), the ideal molecular probe for PMI should have high optical absorption coefficient to enhance the photoacoustic signal. In addition, since the laser output energy is unstable, a photodiode was used to monitor and calibrate the intensity and stability of the laser beam.

4　Conclusion

The use of PAM for the specific detection of bioconjugated FA-AuNRs has been demonstrated in HeLa cells. FA-AuNRs can be internalized by targeted FR-expressing cells *via* a ligand-receptor-mediated endocytosis pathway. FA-AuNRs were precisely mapped by PAM in a single cell. The results reveal that information about the surface molecules of cancer cells can be obtained using photoacoustic techniques with the aid of specific targeting, that enables the visualization, characterization, and quantification of biological processes at the cellular and subcellular level.

References

[1] Nguyen V P, Li Y, Henry J, *et al*. High resolution multimodal photoacoustic microscopy and optical coherence tomography visualization of choroidal vascular occlusion. Int J Mol Sci, 2020, **21**(18): 6508

[2] Jiang X L, Chen Z J, Xing D. Super-resolution photoacoustic imaging based on saturation difference of transient absorption. Opt Laser Eng, 2022, **150**: 106877

[3] Fu Q, Zhu R, Song J, *et al*. Photoacoustic imaging: contrast agents and their biomedical applications. Adv Mater, 2019, **31**(6): e1805875

[4] Threard T, De Lima Savi E, Avanesyan S, *et al*. Photoacoustic 3-D imaging of polycrystalline microstructure improved with transverse acoustic waves. Photoacoustics, 2021, **23**: 100286

[5] Xiao S Y, Tang Y F, Lin Y M, *et al*. *In vivo* nano contrast-enhanced photoacoustic imaging for dynamically lightening the molecular changes of rheumatoid arthritis. Mater Design, 2021, **207**: 109862

[6] Derouin K, Nguyen V P, Li Y X, *et al*. Multimodal photoacoustic microscopy and OCT molecular imaging of choroidal neovascularization in rabbits using indocyanine green. Invest Ophth Vis Sci, 2021,**62**: 366

[7] Qiu C, Bai Y, Yin T, *et al*. Targeted imaging of orthotopic prostate cancer by using clinical transformable photoacoustic molecular probe. BMC Cancer, 2020, **20**(1): 419

[8] Nyayapathi N, Xia J. Photoacoustic imaging of breast cancer: a mini review of system design and image features. J Biomed Opt, 2019, **24**(12): 1-13

[9] Leng X D, Uddin K M S, Chapman W, *et al*. Assessing rectal cancer treatment response using coregistered endorectal photoacoustic and US imaging paired with deep learning. Radiology, 2021, **299**(2):349-358

[10] Nguyen V P, Qian W, Li Y, *et al*. Chain-like gold nanoparticle clusters for multimodal photoacoustic microscopy and optical coherence tomography enhanced molecular imaging. Nat Commun, 2021, **12**(1): 34

[11] Nguyen T P, Nguyen V T, Mondal S, *et al*. Improved depth-of-field photoacoustic microscopy with a multifocal point transducer for biomedical imaging. Sensors (Basel), 2020, **20**(7): 2020

[12] Shi J, Wong T T W, He Y, *et al*. High-resolution, high-contrast mid-infrared imaging of fresh biological samples with ultraviolet-localized photoacoustic microscopy. Nat Photonics, 2019, **13**: 609-615

[13] Zhong J, Wen L, Yang S, *et al*. Imaging-guided high-efficient photoacoustic tumor therapy with targeting gold nanorods. Nanomedicine, 2015, **11**(6): 1499-1509

[14] Li B, Qin H, Yang S, *et al*. *In vivo* fast variable focus photoacoustic microscopy using an electrically tunable lens. Opt Express, 2014, **22**(17): 20130-20137

[15] Huang J, Pu K. Activatable molecular probes for second near-infrared fluorescence, chemiluminescence, and photoacoustic imaging. Angew Chem Int Ed Engl, 2020, **59**(29): 11717-11731

[16] Nguyen V P, Qian W, Wang X, *et al*. Functionalized contrast agents for multimodality photoacoustic microscopy, optical coherence tomography, and fluorescence microscopy molecular retinal imaging. Methods Enzymol, 2021, **657**: 443-480

[17] Xu Y, Li C, Xu R, *et al*. Tuning molecular aggregation to achieve highly bright AIE dots for NIR-II fluorescence imaging and NIR-I photoacoustic imaging. Chem Sci, 2020, **11**(31): 8157-8166

[18] Wang J J, Hu Q K, Li M Z, *et al*. Poly(3-hexylthiophene)/gold nanorod composites as efficient hole-transporting materials for perovskite solar cells. Sol Rrl, 2020, **4**: 2070066

[19] Liu Y, Tan M, Fang C, *et al*. A novel multifunctional gold nanorod-mediated and tumor-targeted gene silencing of GPC-3 synergizes photothermal therapy for liver cancer. Nanotechnology, 2021, **32**(17): 175101

[20] Mousavi S M, Hashemi S A, Mazraedoost S, *et al*. Multifunctional gold nanorod for therapeutic applications and pharmaceutical delivery considering cellular metabolic responses, oxidative stress and cellular longevity. Nanomaterials (Basel), 2021, **11**(7): 1868

[21] Chen Y S, Zhao Y, Yoon S J, *et al*. Miniature gold nanorods for photoacoustic molecular imaging in the second near-infrared optical window. Nat Nanotechnol, 2019, **14**(5): 465-472

[22] Requejo K I, Liopo A V, Zubarev E R. Gold nanorod synthesis with small thiolated molecules. Langmuir, 2020, **36**(14): 3758-3769

[23] Cao W, Wang X D, Song L, *et al*. Folic acid-conjugated gold nanorod@polypyrrole@Fe_3O_4 nanocomposites for targeted MR/CT/PA multimodal imaging and chemo-photothermal therapy. RSC Adv, 2019, **9**(33): 18874-18887

[24] Liu J, Ma W, Kou W, *et al*. Poly-amino acids coated gold nanorod and doxorubicin for synergistic photodynamic therapy and chemotherapy in ovarian cancer cells. Biosci Rep, 2019, **39**(12): BSR20192521

[25] Wang J, Zhu C, Han J, *et al*. Controllable synthesis of gold nanorod/conducting polymer core/shell hybrids toward *in vitro* and *in vivo* near-infrared photothermal therapy. ACS Appl Mater Interfaces, 2018, **10**(15): 12323-12330

[26] Decarlo A, Malardier-Jugroot C, Szewczuk M R. Folic acid-functionalized nanomedicine: folic acid conjugated copolymer and folate receptor interactions disrupt receptor functionality resulting in dual therapeutic anti-cancer potential in breast and prostate cancer. Bioconjug Chem, 2021, **32**(3): 512-522

[27] Zhang D Y, Zheng Y, Zhang H, *et al*. Folate receptor-targeted theranostic IrSx nanoparticles for multimodal imaging-guided combined chemo-photothermal therapy. Nanoscale, 2018, **10**(47): 22252-22262

[28] Angelopoulou A, Kolokithas-Ntoukas A, Fytas C, *et al*. Folic acid-functionalized, condensed magnetic nanoparticles for targeted delivery of doxorubicin to tumor cancer cells overexpressing the folate receptor. ACS Omega, 2019, **4**(26): 22214-22227

[29] Zhou Y, Yao J, Maslov K I, *et al*. Calibration-free absolute quantification of particle concentration by statistical analyses of photoacoustic signals *in vivo*. J Biomed Opt, 2014, **19**(3): 37001

叶酸受体靶向的金纳米棒用于细胞内光声成像*

钟俊平[1)**]　陈金莺[2)**]

（[1)] 佛山科学技术学院物理与光电工程学院粤港澳智能微纳光电技术联合实验室，佛山 528225；
[2)] 暨南大学第一附属医院眼科，广州 510632）

摘要　目的　分子成像技术具有“早期检测”的特点，由于分子水平上的畸变早于解剖水平上的变化。本研究采用细胞内光声分子成像（PMI）方法，对靶向到癌细胞上的叶酸-金纳米棒（FA-AuNRs）精确定位成像。**方法**　本文合成了FA-AuNRs，并对其性质包括形貌、吸收光谱和生物相容性进行了研究。修饰叶酸赋予FA-AuNRs特异性靶向到叶酸受体高表达癌细胞的能力。然后，通过PMI实验研究FA-AuNRs对癌细胞的靶向特异性。**结果**　FA-AuNRs呈棒状，在~800 nm处有一近红外吸收峰。在癌细胞的细胞质中观察到强光声信号，而在正常细胞中只有弱光声信号，表明FA-AuNRs通过叶酸受体介导的内吞作用被癌细胞选择性摄取。这项研究证明了PMI能够实现对靶向到癌细胞上的FA-AuNRs精确定位成像。**结论**　借助特异性靶向作用，可以通过PMI获得癌细胞表面分子信息。该方法有望实现在细胞和分子水平上对生物过程进行可视化、表征和量化。

关键词　分子成像，纳米粒子，金纳米棒，光声成像
中图分类号　O43，Q81　　**DOI**：10.16476/j.pibb.2022.0136

* 国家自然科学基金（61705036），中央高校基本科研业务费专项资金（21621052），广东省医学科研基金（A2022415）和粤港澳智能微纳光电技术联合实验室（2020B1212030010）资助项目。
** 通讯联系人。
钟俊平　Tel：13268286089，E-mail：zjp85@126.com
陈金莺　Tel：15017541741，E-mail：chenjy0907@126.com
收稿日期：2022-04-02，接受日期：2022-06-30